Carbohydrate Polymers 83 (2011) 1908–1915

Contents lists available at ScienceDirect

Carbohydrate Polymers

journal homepage: www.elsevier.com/locate/carbpol

Green fabrication of chitosan films reinforced with parallel aligned graphene oxide

Yongzheng Pan, Tongfei Wu, Hongqian Bao, Lin Li*

School of Mechanical and Aerospace Engineering, Nanyang Technological University, 50 Nanyang Avenue, Singapore 639798, Singapore

ARTICLE INFO

Article history:
Received 15 July 2010
Received in revised form
28 September 2010
Accepted 25 October 2010
Available online 30 October 2010

Keywords:
Chitosan
Graphene oxide
Nanocomposites
Mechanical properties

ABSTRACT

The excellent water solubility of graphene oxide (GO) imparts it feasibility as a new filler for reinforcing hydrophilic biopolymers. In this work, we present a simple and green approach to fabrication of GO/chitosan nanocomposite films. Mechanical properties of the nanocomposite have been significantly enhanced without sacrificing the optical transparency. GO sheets are unidirectionally aligned in the chitosan matrix and parallel to the surface of nanaocomposite film, which has been manifested by the morphological observation and explained by the theoretical prediction of tensile modulus. With incorporation of 1 wt% GO, the fracture strength and tensile modulus of the nanocomopsites are significantly enhanced by 93% and 51%, respectively. The simultaneous improvement of strength and toughness could be attributed to the homogeneous dispersion and alignment of GO sheets in the chitosan matrix, the strong interfacial adhesion between GO and chitosan, as well as the high specific surface area and the two-dimensional geometry of GO.

1. Introduction

Graphene, a single layer of carbon atoms in a closely packed honeycomb two-dimensional lattice, has attracted considerable attention from both experimental and theoretical scientific communities in recent years (Geim & Novoselov, 2007; Rao et al., 2009; Stankovich et al., 2006). Due to its extraordinary mechanical, electronic and thermal properties, graphene has opened new pathways for developing a wide range of novel functional materials. Perfect graphene does not exist naturally, but bulk and solution-processable functionalized graphene materials including graphene oxide (GO) can now be prepared (Hao, Qian, Zhang, & Hou, 2008; Li, Muller, Gilje, Kaner, & Wallace, 2008; Park et al., 2008; Park & Ruoff, 2009; Stankovich et al., 2007). Oxygen functional groups (e.g. hydroxyl, epoxide, and carbonyl groups) attached on the basal planes and edges of GO sheets significantly alter the van der Waals interactions between the layers of graphene and impart the desired solubility in water and some organic solvents (Paredes, Villar-Rodil, Martinez-Alonso, & Tascon, 2008), which provides a convenient access to fabrication of graphene-based materials by solution casting. Meanwhile, these polar functional groups modify surface of graphene to improve interfacial interaction between GO and a hydrophilic polymer. Recent studies have shown that GO can be dispersed throughout a selected polymer matrix to make GO-based nanocomposites with excellent mechanical and thermal properties (Fang, Wang, Lu, Yang, & Nutt, 2009; Liang et al., 2009; Prasad, Das, Maitra, Ramamurty, & Rao, 2009; Villar-Rodil, Paredes, Martinez-Alonso, & Tascon, 2009; Xu, Hong, Bai, Li, & Shi, 2009). Meanwhile, GO sheets have also been attempted to make functional biomaterials (Chen, Müller, Gilmore, Wallace, & Li, 2008; Park et al., 2010; Xu, Bai, Lu, Li, & Shi, 2008). Chen et al. reported that the GO paper was nonhemolytic and noncytotoxic to some mammalian cell lines (Chen et al., 2008). Thus, GO sheets have a great potential in application as reinforcing fillers with effective cost to fabricate biocompatible nanocomposite materials.

Chitosan is one of the second abundant natural biopolymers on the earth. It has been extensively investigated for several decades for biosensors, separation membrane, artificial skin, bone substitutes, water treatment, and so on, because of its biocompatibility, biodegradability, multiple functional groups, as well as its solubility in aqueous medium (Fernandes et al., 2010; Kurita, 2001; Liu, Qin, He, & Song, 2009a). However, despite numerous advantages and unique properties of chitosan, its mechanical properties are not good enough to satisfy a wide range of applications. The formation of organic–inorganic hybrids through incorporation of fillers is an effective approach for improving physical and mechanical properties of chitosan. For example, hydroxyapatite (Cai et al., 2009), cellulose whiskers (Li, Zhou, & Zhang, 2009; Shih, Shieh, & Twu, 2009), clay (Darder, Colilla, & Ruiz-Hitzky, 2003; Wang, Chen, & Tong, 2006; Wang et al., 2005a; Wang, Shen, Zhang, & Tong, 2005b) and carbon nanotubes (Liu, Chen, & Chang, 2009b; Tang et al., 2008; Wang et al., 2005b) have been used to reinforce chitosan. Yang et al. recently studied the nanocomposites of chitosan and graphene oxide (GO) in aqueous media (Yang, Tu, Li, Shang, & Tao, 2010). In

* Corresponding author. Tel.: +65 6790 6285; fax: +65 6791 1859.
E-mail address: mlli@ntu.edu.sg (L. Li).

0144-8617/$ – see front matter © 2010 Elsevier Ltd. All rights reserved.
doi:10.1016/j.carbpol.2010.10.054

their work, with incorporation of 1 wt% graphene oxide, the tensile strength and Young's modulus of GO/chitosan nanocomposites were improved by 122% and 64%, respectively. They considered that the GO sheets might be dispersed well with an orientation in the chitosan matrix, but no strong experimental evidence for the alignment of GO sheets has been shown in the paper.

In the present study, we report the preparation and characterization of novel transparent GO/chitosan nanocompsoite films by means of a simple and fully green method, that is, casting a suspension of GO in an aqueous solution of chitosan. Because GO sheets contain abundant oxygen groups and chitosan contains amino and hydroxyl groups, a homogeneous dispersion of GO into chitosan and strong interfacial adhesions between them can be achieved. A significant reinforcement by GO has been observed for these GO/chitosan nanocomposites from the increases in tensile strength, tensile modulus and elongation at break. Furthermore, the analysis of mechanical properties by utilizing the Halpin–Tsai model and the directly observed morphological structures by field emission scanning electron microscopy (FESEM) have nicely supported the reinforcing mechanism that the GO sheets were parallel to the surface of nanaocomposite films.

2. Experimental

2.1. Materials

Chitosan powder from crab shell, with a deacetylation degree of 87.0% and viscosity-average molecular weight of 186,000 g/mol, was bought from Zhejiang Golden-Shell Biochemical Co. Ltd. (Yuhuan, China). Graphite with an average particle size of 100 μm was obtained from Fluka. All other reagents and chemicals were of analytic grade and used as received.

2.2. Preparation of graphene oxide (GO)

Graphene oxide was synthesized using a modified Hummer's method from natural graphite powder (Hummers & Offeman, 1958; Kovtyukhova et al., 1999). Graphite powder (3 g) was put into an 80 °C solution of concentrated H_2SO_4 (12 mL), $K_2S_2O_8$ (2.5 g), and P_2O_5 (2.5 g). The mixture was kept at 80 °C for 6 h using a hotplate. Successively, the mixture was cooled to room temperature and diluted with 0.5 L of de-ionized water and left to overnight. Then the mixture was filtered and washed with de-ionized water using a 0.2 μm Nylon filter to remove the residual acid. The product was dried under ambient condition overnight. This pre-oxidized graphite was then subjected to oxidation by the Hummers' method (Hummers & Offeman, 1958). Briefly, 1 g of pretreated graphite and 0.5 g of $NaNO_3$ were placed in a flask. Then, 25 mL of H_2SO_4 was added with stirring in an ice-water bath, and 3 g of $KMnO_4$ were slowly added over about 1 h. Stirring was continued for 2 h in the ice-water bath. After the mixture was stirred vigorously for 2 days at room temperature, 100 mL of 5 wt% H_2SO_4 aqueous solution was added over about 1 h with stirring, and the temperature was kept at 98 °C. The resultant mixture was further stirred for 2 h at 98 °C. The temperature was reduced to 60 °C, 3 mL of H_2O_2 (30 wt% aqueous solution) was added, and the mixture was stirred for 2 h at room temperature. The oxidation product was purified by rinsing with a 10% HCl solution, repeatedly washing with copious amounts of de-ionized water, and filtering through a 0.2 μm Nylon filter.

2.3. Preparation of GO/chitosan nanocomposites

The 1 wt% chitosan solution was prepared by dissolving chitosan in 2% (v/v) aqueous acetic acid solution using a magnetic stirrer at 200 rpm for 1 h and filtered with a filter paper to remove the impurity under vacuum. Subsequently, a desired amount of GO suspension (0.1 mg/mL) was added into the chitosan solution. The solution was then stirred at 200 rpm for 1 h, followed by sonication for 10 min to remove the bubbles. After that, the GO/chitosan suspension was poured into a plastic dish and placed in fume hood at room temperature to allow water to evaporate to form a film, followed by drying in a vacuum oven at 50 °C for 24 h. The films containing 0, 0.25, 0.5, 0.75, 1 wt% GO were prepared and cut into test samples using a razor blade and kept in an oven at 50 °C for 2 h before mechanical testing.

2.4. Characterization

The atomic force microscopic (AFM) measurements with the typical tapping-mode were performed using Digital Instrument S3000 AFM. The samples for AFM were prepared by dropping an aqueous GO solution (~0.01 mg/mL) onto a fresh silicon wafer, followed by drying in air.

The transmission electron microscopic (TEM) imaging of GO sheets was done on a JEOL 2010 TEM. The samples were prepared as follows. After being sonicated for 5 min with an ultrasonic bath cleaner, a droplet of aqueous GO dispersion was cast onto a TEM copper grid and the solvent was evaporated overnight at room temperature.

The Fourier transform infrared (FTIR) spectra for a thin film of GO were recorded on a Nicolet 5700 FTIR instrument with attenuated total reflectance (ATR) accessory.

For the surface chemistry analysis, a Kratos Ultra X-ray photoelectron spectroscopy (XPS) system was used with a monochromatic Al Ka X-ray source operating at 15 kV and 10 mA. The corelevel spectra were obtained at a photoelectron take-off angle of 90°, measured with respect to the sample surface.

Ultraviolet–visible spectrometry (UV–vis, Varian Cary 50 Bio Spectrophotometer) was used to examine the effect of GO sheets on the light transmittance of GO/chitosan films. For each sample three different places were randomly chosen for wavelength scanning, to examine the dispersion state of GO sheets in the polymer. The wavelength range was from 200 nm to 800 nm.

The wide-angle X-ray diffraction (XRD) patterns of GO and GO/chitosan films were recorded using a Bruker GADDS diffractometer with an area detector operating under a voltage of 40 kV and a current of 40 mA using Cu Kα radiation ($\lambda = 0.15418$ nm).

The tensile properties of cast samples (dimension 20 mm × 5 mm with varying thickness) were measured using an Instron Model 5543 mechanical tester at room temperature. A 100 N load cell was used and the strain rate was 5.0 mm/min. To ensure data accuracy and repeatability, at least 5 measurements were carried out for each nanocomposite.

The morphology of nanocomposite films was observed using field emission scanning electron microscopy (FESEM, JEOL JSM-6700F). Samples were fractured in liquid nitrogen, and sputtered with gold before observation.

Rheological tests were conducted for the aqueous solutions of neat chitosan, 0.5 wt% GO/chitosan, and 1 wt% GO/chitosan using a fluid rheometer (ARES 100FRTN1, Rheometric Scientific) with a parallel plate of 50 mm diameter. The concentrations of chitosan in all samples were fixed at 40 mg/mL. The storage modulus (G') and loss modulus (G'') were measured as a function of angular frequency at 25 °C.

3. Results and discussion

3.1. Exfoliation and dispersion of graphene oxide

The size and thickness information for the as-prepared GO sheets were fully obtained by AFM and TEM (Fig. 1). A GO sheet is supposed to be thicker than an ideal atomically flat graphene sheet which has a well-known thickness of 0.34 nm, due to the presence

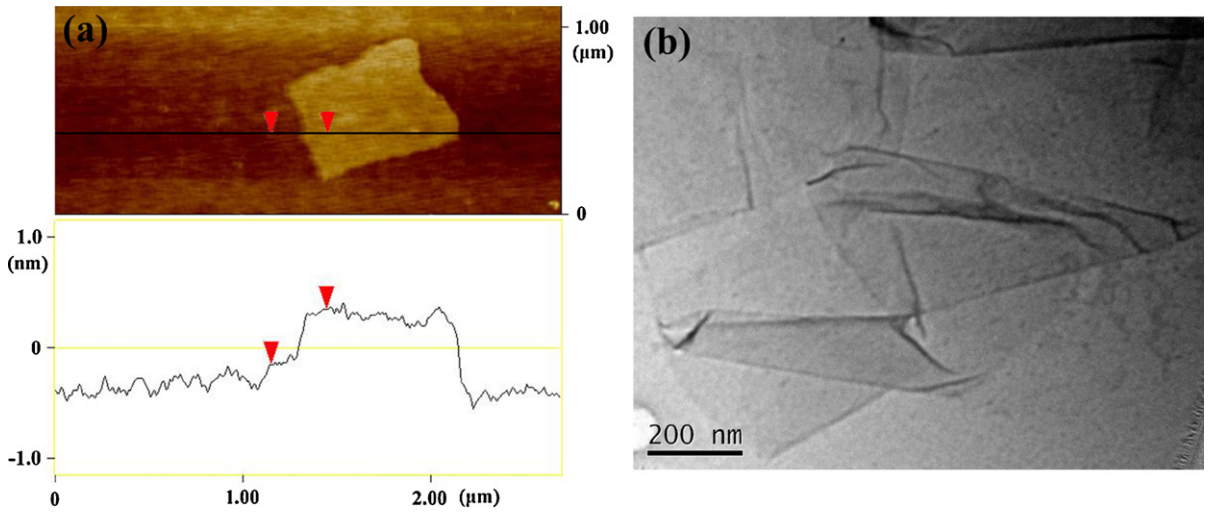

Fig. 1. (a) Tapping mode AFM image of GO sheet and (b) TEM image of GO sheet.

of functionalized groups on both sides of GO sheets and their defects introduced by the oxidation process. In some cases, the thickness of a GO sheet is even larger than 0.8 nm as predicted by the theory (Schniepp et al., 2006). As shown in Fig. 1(a), the measured thickness of the GO sheets was very uniform (~0.6–0.8 nm), suggesting the complete exfoliation of GO sheets down to individual ones. The TEM results also verified the existence of individual GO sheets in water. Fig. 1(b) shows a typical TEM picture indicating that GO was fully exfoliated into individual sheets by ultrasonic treatment.

The information on the functionalized groups on GO surface due to the oxidation process can be obtained from FTIR (Fig. 2(I)). The peaks at 1057 cm^{-1}, 1379 cm^{-1}, 1614 cm^{-1}, 1726 cm^{-1}, 3147 cm^{-1}

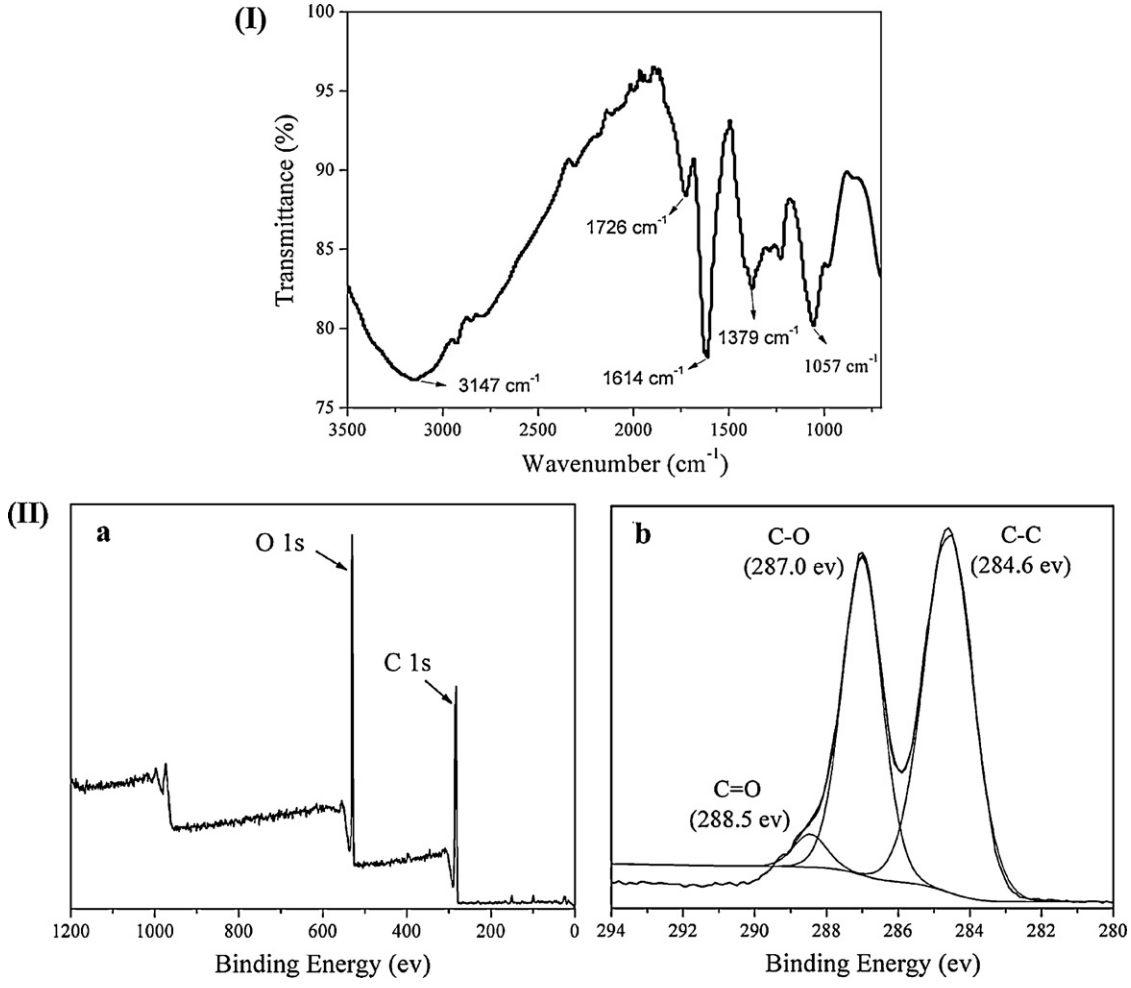

Fig. 2. (I) FTIR spectrum of GO. (II) (a) XPS survey scan spectrum and (b) deconvoluted XPS C 1s spectra of GO.

can be attributed to C–O (ν (epoxy or alkoxy)), O–H (ν (carboxyl)), C=C assigning to skeletal vibrations of unoxidized graphite domains, C=O in carboxylic acid and carbonyl moieties, and O–H (broad coupling ν (hydroxyl)) (Guo, Wang, Qian, Wang, & Xia, 2009), respectively. The abundant oxygen functional groups make GO sheets strongly hydrophilic, which improves their solubility in water. The high degree of functionalization on GO was also confirmed by XPS: the survey spectra for pristine graphite (not shown) and GO yielded C/O atomic ratios of 99 and 2.5, respectively. The XPS survey spectra and C 1s spectra of GO are presented in Fig. 2(II) (a) and (b), respectively. From the C 1s XPS spectra of GO, the two maximum peaks in the C 1s band of Fig. 2(II) (b) are separated by ~2 eV (Schniepp et al., 2006), which is in agreement with the results in the literature for similar C 1s band shapes. The C 1s band can be fitted to three components, which clearly indicated a considerable degree of oxidation, corresponding to carbon atoms in different functional groups: C–C (284.6 eV), C–O (287.0 eV) and C=O (288.5 eV), respectively (Paredes et al., 2008; Stankovich et al., 2007).

The GO/chitosan nanocomposites were prepared by a solution-casting method. The distribution of GO sheets in the chitosan matrix is largely influenced by their dispersion state in the water. A good and stable dispersion of the GO in water and in an aqueous chitosan solution is clearly evident from the photographs shown in Fig. 3(I) (a) and (b) which were taken two weeks later after the ultrasonic dispersion. The dispersion stability of the GO sheets in water and in the chitosan solution may be attributed to the hydrophilicity and compatibility of GO sheets with chitosan due to the oxygen functional groups on GO sheets. This homogeneous aqueous suspension of GO provides us with a promising way for making uniform and high-performance nanocomposite films. The photographs of GO/chitosan composite films with different GO contents are shown in Fig. 3(I) (c)–(g). All the GO/chitosan composite films are smooth, uniform and transparent. With increasing GO content, the color of composite films gradually changes from colorless to brown.

The dispersion uniformity of GO in the chitosan matrix was further examined by UV–vis transmittance measurement over a wavelength range of 280 to 800 nm and XRD characterization. Fig. 3(II) displays the variation in UV–vis transmittance of chitosan films with increasing GO content. Clearly, the light transmittance of the films continuously decreases with increasing GO content, but these nanocomposite films still maintain favorable optical transparency. For the neat chitosan film, the light transmittance at 800 nm is 91% and decreases to 70% as the GO content of composites is increased to 1 wt%. The linear decrease in light transmittance with the GO content is indicative of the uniform dispersion of GO in the matrix, especially when the measurements at different locations of a nanocomposite film reveal the similar light transmittances at a given wavelength. Fig. 3(III) shows the XRD spectra for neat GO, neat chitosan, and 1 wt% GO/chitosan nanocomposite. The characteristic XRD peak of neat GO sheets appears at $2\theta = 8.6^\circ$. The neat chitosan does not show any clear peaks in XRD, indicating its amorphous structure. The XRD pattern of 1 wt% GO/chitosan nanocomposite is nearly the same as the neat chitosan, implying that GO sheets were well exfoliated in the chitosan matrix and the amorphous structure of chitosan was not affected by the incorporation of GO. Apparently, the results of UV–vis and XRD spectrum both suggest that GO sheets have been dispersed in the chitosan matrix homogeneously, which should lead to significant improvement in mechanical properties of filled polymer nanocomposites.

3.2. Mechanical properties and reinforcement mechanism of GO/chitosan nanocomposites

Given the excellent elastic modulus (~1 TPa) and intrinsic strength (125 GPa) of graphene (Lee, Wei, Kysar, & Hone, 2008), we

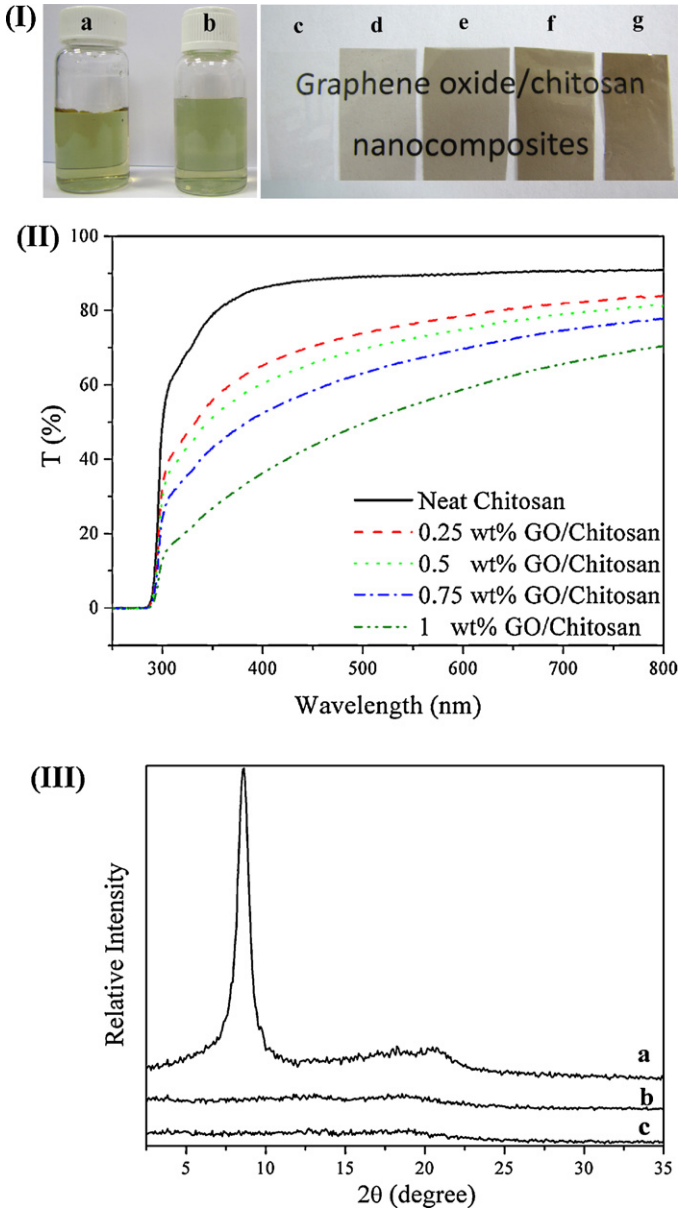

Fig. 3. (I) Photographs of (a) GO aqueous solution, (b) GO/chitosan aqueous solution, (c) neat chitosan film, (d) 0.25 wt%, (e) 0.5 wt%, (f) 0.75 wt% and (g) 1 wt% GO/chitosan composite films. (II) UV–vis spectra of neat chitosan and GO/chitosan composite films. (III) XRD patterns of (a) neat GO, (b) 1 wt% GO/chitosan nanocomposite, and (c) neat chitosan.

examine the effect of GO sheets on mechanical properties of chitosan films. Fig. 4(a) shows the representative stress–strain curves for neat chitosan and GO/chitosan nanocomposite films. The tensile strength, elongation at break and tensile modulus as a function of GO content are plotted in Fig. 4(b) and (c). The mechanical properties of all samples tested are summarized in Table 1. All the neat chitosan film and GO/chitosan nanocomposite films show a typical yield behavior in the vicinity of 2% strain. The neat chitosan possesses tensile modulus (E) of 2.92 GPa, fracture strength (σ_s) of 69.1 MPa, and elongation at break of 22.9%. The addition of GO into chitosan films significantly enhanced their E and σ_s. For example, the incorporation of 1 wt% GO increased the E_Y and σ_s to 4.42 GPa and 133.1 MPa, corresponding to the increases by 51% and 93%, respectively (relative to neat chitosan). The elongation at break was also increased to 31.6%, corresponding to an increase by 41%. The toughness, calculated from the area under the stress–strain curve,

Table 1
Mechanical properties of neat chitosan and GO/chitosan nanocomposites.

Samples	Tensile modulus (GPa)	Tensile strength (MPa)	Elongation at break (%)
Neat chitosan	2.92 ± 0.13	69.1 ± 4.1	22.5 ± 1.5
0.25 wt% GO/chitosan	3.45 ± 0.07	87.5 ± 2.5	22.9 ± 1.7
0.5 wt% GO/chitosan	3.89 ± 0.12	88.9 ± 3.3	24.0 ± 1.6
0.75 wt% GO/chitosan	4.11 ± 0.08	112.2 ± 4.5	29.1 ± 2.3
1 wt% GO/chitosan	4.42 ± 0.15	133.1 ± 6.8	31.6 ± 3.1

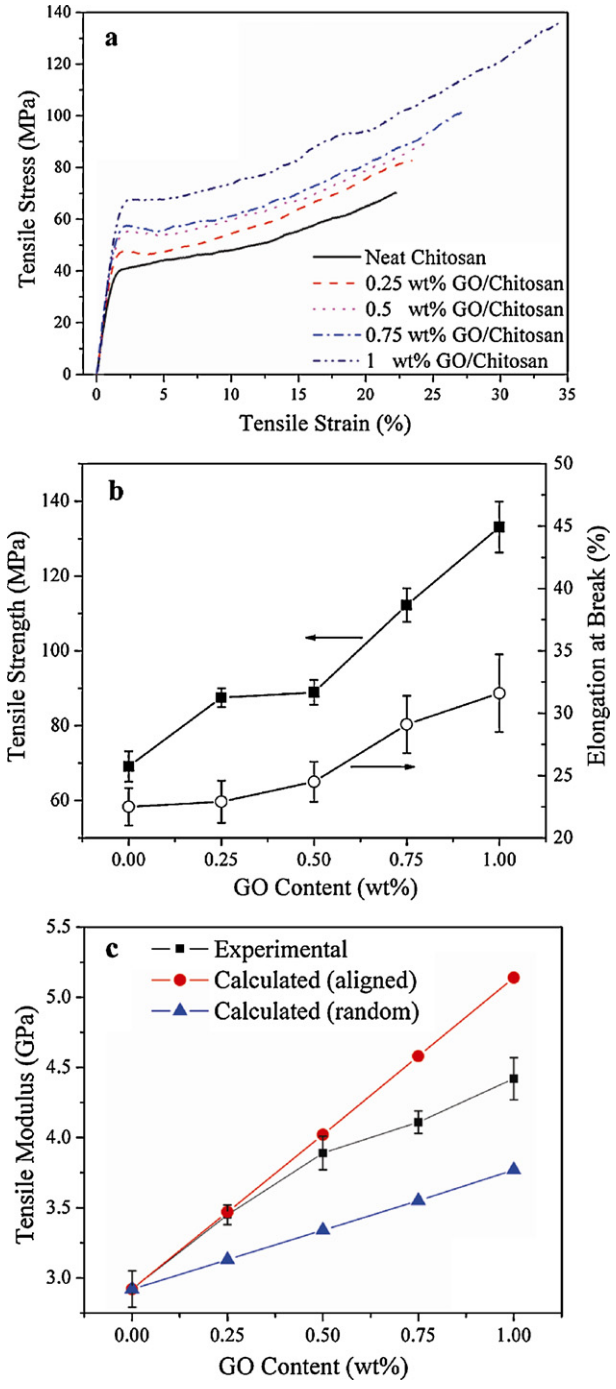

Fig. 4. (a) Tensile stress versus strain curves; (b) tensile strength and elongation at break for GO/chitosan nanocomposites as a function of GO content; (c) experimental tensile modulus and theoretical modulus calculated using the Halpin–Tsai model under the hypothesis that GO sheets are randomly dispersed and aligned in a polymer matrix.

of 1 wt% GO/chitosan films is around 1.6 times higher than that of the neat chitosan film.

The well-established Halpin–Tsai model, which was widely utilized to predict the modulus of unidirectional or randomly distributed filler-reinforced nanocomposites (Gao et al., 2005; Schaefer & Justice, 2007; Zhao, Zhang, Chen, & Lu, 2010), was used in our work to simulate the modulus of the GO/chitosan nanocomposites. For randomly oriented or unidirectional GO sheets in a polymer matrix, the nanocomposites modulus E_c and $E_{//}$ are given by

$$E_c = E_m\left[\frac{3}{8}\frac{1+\eta_L\xi V_c}{1-\eta_L V_c}+\frac{5}{8}\frac{1+2\eta_T V_c}{1-\eta_T V_c}\right] \quad (1)$$

$$E_c = E_m\left[\frac{1+\eta_L\xi V_c}{1-\eta_L V_c}\right] \quad (2)$$

$$\eta_L = \frac{(E_g/E_m)-1}{(E_g/E_m)+\xi} \quad (3)$$

$$\eta_T = \frac{(E_g/E_m)-1}{(E_g/E_m)+2} \quad (4)$$

$$\xi = \frac{2\alpha_g}{3} = \frac{2l_g}{3t_g} \quad (5)$$

where E_c and $E_{//}$ represent the Young's modulus of a nanocomposite with randomly distributed GO and the Young's modulus of the nanocomposite with GO aligned parallel to the surface of a sample film, respectively. E_g and E_m are the Young's modulus of the GO and the polymer matrix respectively. α_g, l_g, and t_g refer to the aspect ratio, length and thickness of a GO sheet respectively, and V_c is the volume fraction of GO in the nanocomposite. The Young's modulus of the GO sheet was previously measured to be around 1 TPa, which is close to that of the graphene used in this work. The Young' modulus of neat chitosan was 2.92 GPa from the experimental result. The density of the chitosan is around 0.7 g/cm^3, and the density of GO is 2.25 g/cm^3. The statistical average l_g and t_g of GO sheets were about 1 μm and 0.8 nm, respectively, as determined by AFM and TEM analysis. Fig. 4(c) shows that the experimentally measured tensile modulus of the nanocompoistes is very close to the theoretically calculated values under the assumption that the GO sheets are unidirectionally aligned and parallel to the surface of the nanocomposite films with a GO content <0.5 wt%. The experimental results begin to deviate from the calculated curve (aligned) and shift toward the curve (random) as the GO content increases. This indicates that the GO sheets are aligned parallel to the surface of the nanocomposites, especially at low GO contents. However, the degree of alignment decrease as the GO content increases, presumably because the higher viscosity of the nanocomposites constrains the motion of GO sheets in the matrix.

The incorporation of GO sheets simultaneously improve the strength and toughness of chitosan films, which was extraordinary as compared with those carbon nanotubes (CNT)/chitosan or nanoclay/chitosan composites reported in the literatures (Li et al., 2009; Wang et al., 2006; Wang et al., 2005b). With incorporation of CNT or nanaclay, elongation at break of composite films decreased, while tensile modulus and strength increased. For example, incorporation of 0.8 wt% multiwalled carbon nanotubes (MWCNTs) resulted in the improvement of tensile modulus

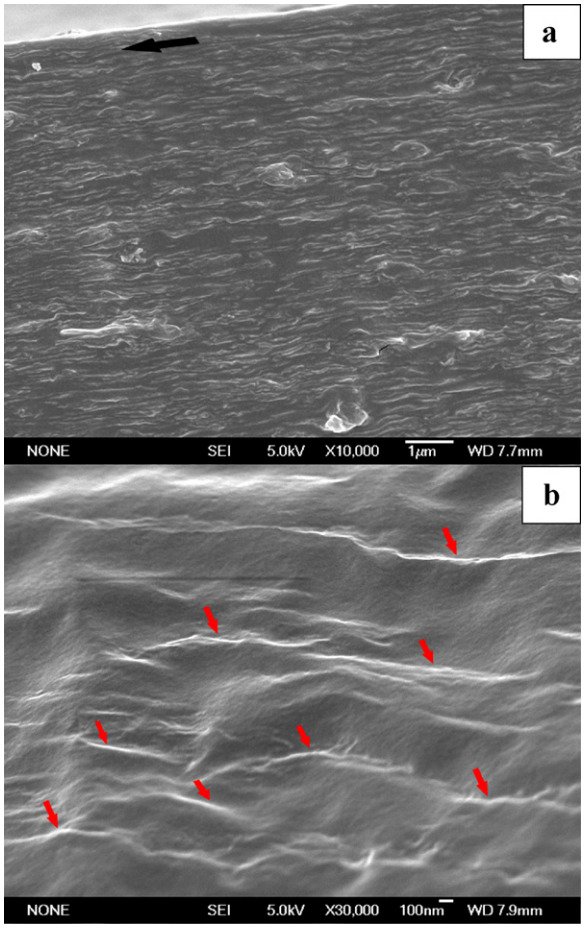

Fig. 5. SEM images of the fractured surface of 1 wt% GO/chitosan nanocomposite film (a) ×10,000 (the black arrow represents the direction of the surface of sample film) and (b) ×30,000 (the red arrows point at the GO sheets).

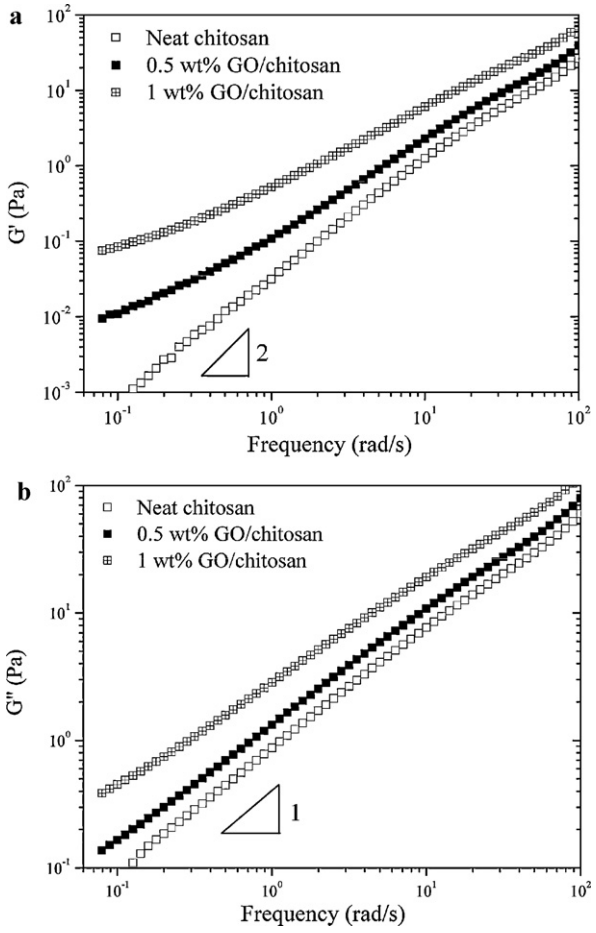

Fig. 6. Frequency response of (a) storage modulus (G′) and (b) loss modulus (G″) for chitosan nanocomposites. The measurement was carried out at 25 °C.

and tensile strength of the nanocomposites by about 93% and 99%, respectively. However, the elongation at break decreased to 13.4%, much lower than that of neat chitosan film (49.5%) (Wang et al., 2005b). Similarly, with addition of 15 wt% cellulose whisker, the tensile strength of the composites films increased from 85 to 120 MPa, while the elongation at break decreased from 20% to only 3% (Li et al., 2009). For our GO/chitosan nanocomposites, the significant reinforcement of chitosan by GO is attributed to the homogeneously dispersed GO sheets throughout the chitosan matrix and the strong interfacial adhesion between GO and chitosan. Chitosan is a hydrophilic biopolymer, which possesses amino, primary, and secondary hydroxyl groups in its glucosamine unit. GO sheets also own superior hydrophilicity because of abundant oxygen functional groups on the surface. Strong hydrogen-bonds may be formed between chitosan and GO sheets. As a result, mechanical properties of chitosan are enhanced significantly by addition of GO.

In particular, as compared with other fillers, GO sheets have higher specific surface area (calculated value, 2630 m^2/g) (Stoller, Park, Zhu, An, & Ruoff, 2008), nanoscale surface roughness and unique two-dimensional (2D) structure. Nanoparticles with high surface area could impose strong geometric constraints to the mobility of polymer molecules, which has been verified by the recent molecular dynamics studies (Ramanathan et al., 2008; Starr, Schroder, & Glotzer, 2002). Likewise, the nanoscale surface roughness may result in an enhanced mechanical interlocking with polymer chains, consequently, leading to better adhesion at the interface. Rafiee et al. have compared the mechanical properties of epoxy nanocomposites filled with graphene platelets, single-walled carbon nanotubes, and multi-walled carbon nanotubes (Rafiee et al., 2009). Their results indicated that graphene platelets significantly outperform carbon nanotubes, which was attributed to the enhanced nanofiller-matrix adhesion/interlocking arising from their wrinkled (rough) surface and two-dimensional geometry of grphene platelets.

To observe the dispersion of GO sheets microscopically for more information concerning the interfacial interaction between the chitosan matrix and GO sheets, the fractured surfaces of composite films were further investigated by FESEM. As shown in Fig. 5(a), GO sheets were uniformly dispersed and embedded into the chitosan matrix, while there a few GO sheets stacked together which might have a negative effect on mechanical reinforcement. Fig. 5(b), an image at a high magnification, shows that no obvious GO sheets were pulled out and the protruding GO sheets were thickly coated with adsorbed polymer, indicating that GO sheets had strong interfacial adhesion with the chitosan matrix. A homogeneous dispersion of GO and efficient interfacial load transfer should result in a uniform stress distribution and be able to minimize the occurrence of stress concentration, leading to a significant increase in mechanical properties of nanocomposites. Apparently, it is observed that GO sheets were unidirectionally distributed in the chitosan matrix and parallel to the surface of sample film, which is exactly in agreement with the result predicted by the Halpin–Tsai model. The alignment of GO sheets probably resulted from the method (i.e. solution casting) used to prepare the nancomposites. GO sheets tended to lie down inside the chitosan solution due to their unique 2D

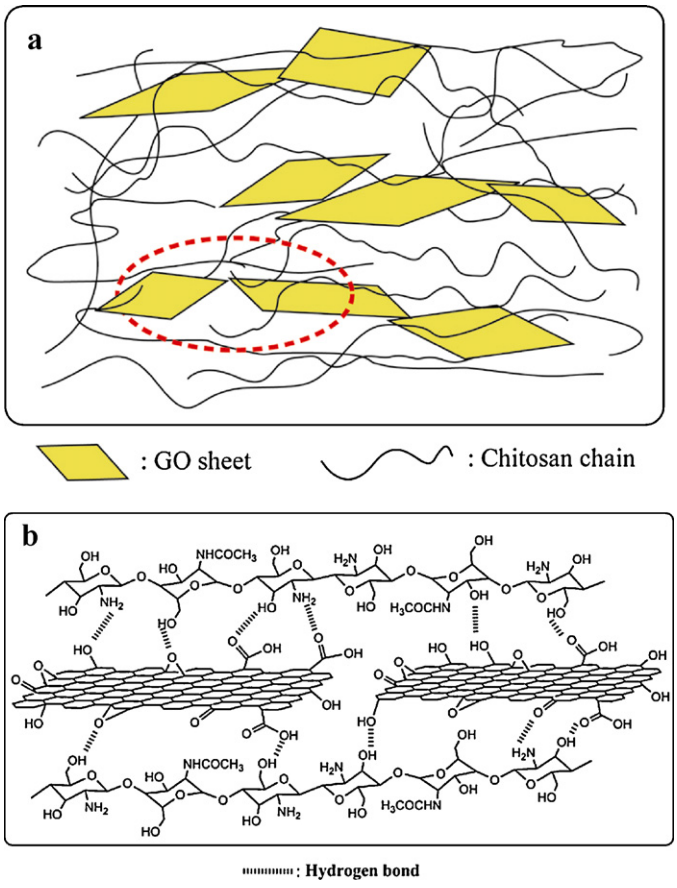

Fig. 7. (a) Scheme for possible microstructure present in GO/chitosan nanocomposites; (b) formation of hydrogen bonds between GO sheets and chitosan chains.

structure and the gravitational attraction. This phenomenon was also found in the preparation of graphite nanoplates/poly(vinylidene fluoride) (He, Lau, Chan, & Fan, 2009) and GO/poly(vinyl alcohol) nanocomposite films (Liang et al., 2009; Xu et al., 2009).

Moreover, the reinforcement of chitosan by GO also possibly arises from an associated GO network. In order to understand the effect of this network on the reinforcementof chitosan, rheological measurements on the concentrated neat chitosan and nanocomposite solutions were carried out. Fig. 6(a) and (b) show the storage modulus G′ and loss modulus G″, respectively, as a function of angular frequency for neat chitosan, 0.5 wt% GO/chitosan and 1 wt% GO/chitosan nanocomposite solutions, where the concentration of chitosan was fixed at 40 mg/mL. In the region of low frequencies (terminal zone), G′ and G″ of the neat chitosan solution typically follow the scaling laws: $G' \sim \omega^1$ and $G'' \sim \omega^2$ (Ferry, 1980). With incorporation of GO, the magnitudes of both storage and loss modulus increase and deviate from the terminal behavior. A plateau-like regime appears, which is indicative of a pseudo-solid-like behavior and the formation of a GO network. Within such a network constituted by the GO sheets, the free movement of polymer chains is restricted and the relaxation of the polymer chains upon the application of low-frequency and low-amplitude strain becomes difficult. The formation of a filler network and strong interaction between GO and chitosan could be important factors for the significant effect of GO on reinforcement of chitosan.

On the basis of mechanical properties and morphologies of the nanocomposites, we schematically propose the possible microstructure of GO/chitosan nanocomposites and the interaction between GO and chitosan, as shown in Fig. 7. In Fig. 7(a), GO sheets are aligned parallel to the surface of nanocomposites film and homogeneously distributed in the chitosan matrix. Fig. 7(b) depicts the possible formation of hydrogen bonds between GO sheets and chitosan chains, representing the circled area in Fig. 7(a). Hydrophilic features of both GO sheets and chitosan impart them favorable compatibility. The homogeneous dispersion and a certain degree of alignment of GO sheets in the chitosan matrix, together with the strong interfacial adhesion between GO and chitosan, significantly enhance the mechanical properties of GO/chitosan nanocomposites.

4. Conclusion

In summary, the high-performance GO/chitosan nanocomposites have been successfully prepared using a simple solution-casting method. GO sheets containing abundant carboxylic and hydroxyl groups can form strong interactions with the chitosan matrix. Homogeneous dispersion of GO sheets in the chitosan matrix and strong interfacial adhesion between them significantly enhanced the mechanical properties of nanocomposites. The nanocomposite films containing 1 wt% GO sheets are strong and ductile. The Young's modulus, tensile strength, and elongation at break are found to increase by 51% and 93% and 41%, respectively, which are much higher than those of neat chitosan films. To the best of our knowledge, this is the first study reporting that chitosan nanocomposites could simultaneously have high strength (>100 MPa) and large elongation at break (30%). By comparing the experimental tensile modulus and the value predicted by the Halpin–Tsai model, we know that GO sheets are aligned parallel to the surface of the sample film within the nanocomposites and this fact has been further verified by FESEM. Meanwhile, it is interesting to note that the optical transparency of all the nanocomposites was still maintained. It is expected that the GO/chitosan nanocomposites may find more important applications such as biomaterials that require largely improved tensile properties.

References

Cai, X., Tong, H., Shen, X. Y., Chen, W. X., Yan, J., & Hu, J. M. (2009). Preparation and characterization of homogeneous chitosan-polylactic acid/hydroxyapatite nanocomposite for bone tissue engineering and evaluation of its mechanical properties. *Acta Biomaterialia*, *5*(7), 2693–2703.

Chen, H., Müller, M. B., Gilmore, K. J., Wallace, G. G., & Li, D. (2008). Mechanically strong, electrically conductive, and biocompatible graphene paper. *Advanced Materials*, *20*(18), 3557–3561.

Darder, M., Colilla, M., & Ruiz-Hitzky, E. (2003). Biopolymer–clay nanocomposites based on chitosan intercalated in montmorillonite. *Chemistry of Materials*, *15*(20), 3774–3780.

Fang, M., Wang, K. G., Lu, H. B., Yang, Y. L., & Nutt, S. (2009). Covalent polymer functionalization of graphene nanosheets and mechanical properties of composites. *Journal of Materials Chemistry*, *19*(38), 7098–7105.

Fernandes, S. C. M., Freire, C. S. R., Silvestre, A. J. D., Pascoal Neto, C., Gandini, A., Berglund, L. A., et al. (2010). Transparent chitosan films reinforced with a high content of nanofibrillated cellulose. *Carbohydrate Polymers*, *81*(2), 394–401.

Ferry, J. D. (1980). *Viscoelastic properties of polymers*. New York: John Wiley & Sons.

Gao, J. B., Itkis, M. E., Yu, A. P., Bekyarova, E., Zhao, B., & Haddon, R. C. (2005). Continuous spinning of a single-walled carbon nanotube-nylon composite fiber. *Journal of the American Chemical Society*, *127*(11), 3847–3854.

Geim, A. K., & Novoselov, K. S. (2007). The rise of graphene. *Nature Materials*, *6*(3), 183–191.

Guo, H. L., Wang, X. F., Qian, Q. Y., Wang, F. B., & Xia, X. H. (2009). A green approach to the synthesis of graphene nanosheets. *Acs Nano*, *3*(9), 2653–2659.

Hao, R., Qian, W., Zhang, L. H., & Hou, Y. L. (2008). Aqueous dispersions of TCNQ-anion-stabilized graphene sheets. *Chemical Communications*, *48*, 6576–6578.

He, F., Lau, S., Chan, H. L., & Fan, J. T. (2009). High dielectric permittivity and low percolation threshold in nanocomposites based on poly(vinylidene fluoride) and exfoliated graphite nanoplates. *Advanced Materials*, *21*(6), 710–714.

Hummers, W. S., & Offeman, R. E. (1958). Preparation of graphitic oxide. *Journal of the American Chemical Society*, *80*(6), 13399.

Kovtyukhova, N. I., Ollivier, P. J., Martin, B. R., Mallouk, T. E., Chizhik, S. A., Buzaneva, E. V., et al. (1999). Layer-by-layer assembly of ultrathin composite films from micron-sized graphite oxide sheets and polycations. *Chemistry of Materials*, *11*(3), 771–778.

Kurita, K. (2001). Controlled functionalization of the polysaccharide chitin. *Progress in Polymer Science*, *26*(9), 1921–1971.

Lee, C., Wei, X. D., Kysar, J. W., & Hone, J. (2008). Measurement of the elastic properties and intrinsic strength of monolayer graphene. *Science*, *321*(5887), 385–388.
Li, D., Muller, M. B., Gilje, S., Kaner, R. B., & Wallace, G. G. (2008). Processable aqueous dispersions of graphene nanosheets. *Nature Nanotechnology*, *3*(2), 101–105.
Li, Q., Zhou, J. P., & Zhang, L. N. (2009). Structure and properties of the nanocomposite films of chitosan reinforced with cellulose whiskers. *Journal of Polymer Science Part B: Polymer Physics*, *47*(11), 1069–1077.
Liang, J. J., Huang, Y., Zhang, L., Wang, Y., Ma, Y. F., Guo, T. Y., et al. (2009). Molecular-level dispersion of graphene into poly(vinyl alcohol) and effective reinforcement of their nanocomposites. *Advanced Functional Materials*, *19*(14), 2297–2302.
Liu, F., Qin, B., He, L., & Song, R. (2009). Novel starch/chitosan blending membrane: Antibacterial, permeable and mechanical properties. *Carbohydrate Polymers*, *78*(1), 146–150.
Liu, Y.-L., Chen, W.-H., & Chang, Y.-H. (2009). Preparation and properties of chitosan/carbon nanotube nanocomposites using poly(styrene sulfonic acid)-modified CNTs. *Carbohydrate Polymers*, *76*(2), 232–238.
Paredes, J. I., Villar-Rodil, S., Martinez-Alonso, A., & Tascon, J. M. D. (2008). Graphene oxide dispersions in organic solvents. *Langmuir*, *24*(19), 10560–10564.
Park, S., An, J. H., Piner, R. D., Jung, I., Yang, D. X., Velamakanni, A., et al. (2008). Aqueous suspension and characterization of chemically modified graphene sheets. *Chemistry of Materials*, *20*(21), 6592–6594.
Park, S., Mohanty, N., Suk, J. W., Nagaraja, A., An, J., Piner, R. D., et al. (2010). Biocompatible, robust free-standing paper composed of a TWEEN/graphene composite. *Advanced Materials*, doi:10.1002/adma.200903611
Park, S., & Ruoff, R. S. (2009). Chemical methods for the production of graphenes. *Nature Nanotechnology*, *4*(4), 217–224.
Prasad, K. E., Das, B., Maitra, U., Ramamurty, U., & Rao, C. N. R. (2009). Extraordinary synergy in the mechanical properties of polymer matrix composites reinforced with 2 nanocarbons. *Proceedings of the National academy of Sciences of the United States of America*, *106*(32), 13186–13189.
Rafiee, M. A., Rafiee, J., Wang, Z., Song, H. H., Yu, Z. Z., & Koratkar, N. (2009). Enhanced mechanical properties of nanocomposites at low graphene content. *Acs Nano*, *3*(12), 3884–3890.
Ramanathan, T., Abdala, A. A., Stankovich, S., Dikin, D. A., Herrera-Alonso, M., Piner, R. D., et al. (2008). Functionalized graphene sheets for polymer nanocomposites. *Nature Nanotechnology*, *3*(6), 327–331.
Rao, C. N. R., Sood, A. K., Subrahmanyam, K. S., & Govindaraj, A. (2009). Graphene: the new two-dimensional nanomaterial. *Angewandte Chemie International Edition*, *48*(42), 7752–7777.
Schaefer, D. W., & Justice, R. S. (2007). How nano are nanocomposites? *Macromolecules*, *40*(24), 8501–8517.
Schniepp, H. C., Li, J. L., McAllister, M. J., Sai, H., Herrera-Alonso, M., Adamson, D. H., et al. (2006). Functionalized single graphene sheets derived from splitting graphite oxide. *Journal of Physical Chemistry B*, *110*(17), 8535–8539.
Shih, C.-M., Shieh, Y.-T., & Twu, Y.-K. (2009). Preparation and characterization of cellulose/chitosan blend films. *Carbohydrate Polymers*, *78*(1), 169–174.
Stankovich, S., Dikin, D. A., Dommett, G. H. B., Kohlhaas, K. M., Zimney, E. J., Stach, E. A., et al. (2006). Graphene-based composite materials. *Nature*, *442*(7100), 282–286.
Stankovich, S., Dikin, D. A., Piner, R. D., Kohlhaas, K. A., Kleinhammes, A., Jia, Y., et al. (2007). Synthesis of graphene-based nanosheets via chemical reduction of exfoliated graphite oxide. *Carbon*, *45*(7), 1558–1565.
Starr, F. W., Schroder, T. B., & Glotzer, S. C. (2002). Molecular dynamics simulation of a polymer melt with a nanoscopic particle. *Macromolecules*, *35*(11), 4481–4492.
Stoller, M. D., Park, S. J., Zhu, Y. W., An, J. H., & Ruoff, R. S. (2008). Graphene-based ultracapacitors. *Nano Letters*, *8*(10), 3498–3502.
Tang, C. Y., Xiang, L. X., Su, J. X., Wang, K., Yang, C. Y., Zhang, Q., et al. (2008). Largely improved tensile properties of chitosan film via unique synergistic reinforcing effect of carbon nanotube and clay. *Journal of Physical Chemistry B*, *112*(13), 3876–3881.
Villar-Rodil, S., Paredes, J. I., Martinez-Alonso, A., & Tascon, J. M. D. (2009). Preparation of graphene dispersions and graphene-polymer composites in organic media. *Journal of Materials Chemistry*, *19*(22), 3591–3593.
Wang, S. F., Chen, L., & Tong, Y. J. (2006). Structure–property relationship in chitosan-based biopolymer/montmorillonite nanocomposites. *Journal of Polymer Science Part A: Polymer Chemistry*, *44*(1), 686–696.
Wang, S. F., Shen, L., Tong, Y. J., Chen, L., Phang, I. Y., Lim, P. Q., et al. (2005). Biopolymer chitosan/montmorillonite nanocomposites: Preparation and characterization. *Polymer Degradation and Stability*, *90*(1), 123–131.
Wang, S. F., Shen, L., Zhang, W. D., & Tong, Y. J. (2005). Preparation and mechanical properties of chitosan/carbon nanotubes composites. *Biomacromolecules*, *6*(6), 3067–3072.
Xu, Y., Bai, H., Lu, G., Li, C., & Shi, G. (2008). Flexible graphene films via the filtration of water-soluble noncovalent functionalized graphene sheets. *Journal of the American Chemical Society*, *130*(18), 5856–5857.
Xu, Y. X., Hong, W. J., Bai, H., Li, C., & Shi, G. Q. (2009). Strong and ductile poly(vinyl alcohol)/graphene oxide composite films with a layered structure. *Carbon*, *47*(15), 3538–3543.
Yang, X. M., Tu, Y. F., Li, L. A., Shang, S. M., & Tao, X. M. (2010). Well-dispersed chitosan/graphene oxide nanocomposites. *ACS Applied Materials & Interfaces*, *2*(6), 1707–1713.
Zhao, X., Zhang, Q. H., Chen, D. J., & Lu, P. (2010). Enhanced mechanical properties of graphene-based poly(vinyl alcohol) composites. *Macromolecules*, *43*(5), 2357–2363.